Power Conditioning of Distribution Networks via Single-Phase Electric Vehicles Equipped

Pirouzi, S.; Aghaei, J.; Niknam, T.; Khooban, M. H.; Dragicevic, Tomislav; Farahmand, H.; Korpås, M.; Blaabjerg, Frede

Published in:
IEEE Systems Journal

DOI (link to publication from Publisher):
10.1109/JSYST.2019.2896408

Publication date:
2019

Document Version
Accepted author manuscript, peer reviewed version

Power Conditioning of Distribution Networks via Single-Phase Electric Vehicles Equipped

Sasan Pirouzi, Jamshid Aghaei, *Senior Member, IEEE*, Taher Niknam, *Member, IEEE*, Mohammad Hassan Khooban, Tomislav Dragicevic, Hossein Farahmand, *Member, IEEE*, Magnus Korpås, *Member, IEEE*, and Frede Blaabjerg, *Fellow, IEEE*

***Abstract*—This paper presents the design of a single-phase electric vehicle (EV) on-board bidirectional charger with the capability of power conditioning. This charger can control its charging/discharging active power based on the demand of EV battery/network or load. Also, it controls reactive power and harmonic current based on the characteristics of the nonlinear and linear loads. The topology of the proposed charger consists of the bidirectional ac/dc and buck–boost dc/dc converters, where it can operate in four quadrants in the active-reactive power plane with the capability of harmonic compensation. In the next step, this paper presents a suitable control strategy for the bidirectional charger according to the instantaneous active and reactive power (PQ) theory. Based on the PQ theory, the active and reactive power that includes average and oscillatory components obtained, based on the demand of nonlinear/linear loads and EV battery. Then, the reference current of ac/dc converter of the charger and battery is obtained, and in the next step, the situation of the charger switches is determined using output signals of the proportional–integral and proportional–resonant controllers and pulsewidth modulation. Finally, the proposed approach is validated and implemented in the OPAL-RT to integrate the fidelity of the physical simulation and the flexibility of the numerical simulations.**

***Index Terms*—Active and reactive power control, bidirectional charger, electric vehicles (EVs), harmonic compensation, power conditioning, three-phase instantaneous active and reactive power (PQ) theory.**

NOMENCLATURE

Acronyms

AC/DC	Alternating/direct current
DISCO	Distribution company
EV	Electric vehicle
FACTS	Flexible ac transmission system
HIL	Hardware-in-loop
ICE	Internal combustion engine
PCC	Point of common coupling
PHEV	Plug-in hybrid electric vehicle
PI	Proportional–integral
PQ	Active-reactive power
PR	Proportional–resonant
PWM	Pulsewidth Modulation
SVC	Static var compensator
THD	Total harmonic distortion

Subindexes

a, b, c	Indices of phase *a*, *b*, *c*
d	Duty cycle
du	Applied signal to PWM in the ac/dc converter
$I_{\rm bt}$, $I^*_{\rm bt}$	Battery current and reference current of battery
IC, $IC^{\rm ref}$	Charger current and reference current of charger
IC^p, IC^q	Active and reactive components of charger current
IL	Consumption and injected harmonic current of EV
K^P, K^I	Proportional and integral coefficients
$P^{\rm app}$, $Q^{\rm app}$	Applied active and reactive power to charger
$P_{\rm avg}$, $Q_{\rm avg}$	Average active and reactive power
PC_u	Required active power of battery from network
P_h, Q_h	Active and reactive power due to harmonic frequency components
PL, QL	Active and reactive power of load
$P_{\rm osc}$, $Q_{\rm osc}$	Oscillatory active and reactive power
$P^{\rm ref}$, $Q^{\rm ref}$	Reference active and reactive power
$P_{2\omega}$, $Q_{2\omega}$	Active and reactive power due to unbalance system (negative and zero sequences)
s	Term of Laplace
$V_{\rm dc}$, $V^*_{\rm dc}$	dc-link voltage and reference dc-link voltage
$V^{\rm ref}_{\rm dc}$	Reference dc-link voltage
$V^{\rm PCC}$	Voltage in the PCC
ω	Network frequency
ω_c	Resonant frequency in the PR controller

Manuscript received February 28, 2018; revised June 25, 2018, September 17, 2018, and December 18, 2018; accepted January 26, 2019. This work was supported by the European Union under the Horizon2020 Framework Programme under Grant 731148 (INVADE H2020 project). *(Corresponding author: Jamshid Aghaei.)*

S. Pirouzi and T. Niknam are with the Department of Electrical and Electronics Engineering, Shiraz University of Technology, Shiraz 71557-13876, Iran (e-mail: s.pirouzi@sutech.ac.ir; niknam@sutech.ac.ir).

J. Aghaei is with the Department of Electrical and Electronics Engineering, Shiraz University of Technology, Shiraz 71557-13876, Iran, and also with the Department of Electric Power Engineering, Norwegian University of Science and Technology, Trondheim NO-7491, Norway (e-mail: aghaei@sutech.ac.ir).

M. Khooban, T. Dragicevic, and F. Blaabjerg are with the Department of Energy Technology, Aalborg University, Aalborg DK-9220, Denmark (e-mail: khooban@ieee.org; tdr@et.aau.dk; fbl@et.aau.dk).

H. Farahmand and M. Korpås are with the Department of Electric Power Engineering, Norwegian University of Science and Technology, Trondheim NO-7491, Norway (e-mail: Hossein.farahmand@ntnu.no; magnus.korpas@ntnu.no).

Digital Object Identifier 10.1109/JSYST.2019.2896408

I. INTRODUCTION

THE electric vehicles (EVs), as alternatives for fossil fuel-based vehicles, are the new technology that is used for decreasing the environmental pollution. The EV includes conventional internal combustion engine and the electrical motor,

in which the required energy of the electrical motor is provided by embedded battery in EV. Also, some of EVs such as plug-in hybrid EVs (PHEVs) are connected to the network to receive required energy for their batteries. But, it is noted that large number of the EV connection to the network will cause increasing concerns and problems in the power system and/or distribution networks [1]–[3]. In addition, the EVs are connected to the network using chargers composed of ac/dc and dc/dc unidirectional converters. Hence, the EVs behave as nonlinear loads in the network, and they may inject harmonics to the network [4], [5]. Also, the presence of the harmonic in the distribution networks causes reduction in the distribution transformers' lifetime and malfunctioning of some equipment [6]–[8]. Moreover, the EVs with unidirectional charger act as passive loads, hence, the large number of EVs' connection to the network causes increased voltage drop and network power loss as well as overloading of distribution lines [9], [10].

To reduce the harmonic injection into the network, researches have proposed to charge EVs by group [11] and change the charger structure [12]–[14]. In [11], the EVs are charged by the group, and accordingly it is proved that the total harmonic distortion (THD) of the EVs has been reduced with respect to the individual charging. Also, in [12]–[14], bidirectional chargers including ac/dc and dc/dc bidirectional converters based on insulated-gate bipolar transistor (IGBT) switches have been proposed. Based on [12]–[14], this charger can control its active and reactive power as well as harmonic current, therefore, the EVs can improve the power quality and network indexes such as voltage. Although the authors of [12]–[14] have proposed EVs to decrease their own currents' harmonics, but there are other nonlinear loads, e.g., six-pulse converters, that cause power quality concerns in power systems. In many research works [15]–[17], Flexible ac transmission system (FACTS) or custom power devices are used to decrease the negative impacts of these nonlinear loads. Also, the FACTS can regulate the voltage at the point of common coupling (PCC) by injecting the reactive power as done in [15] and [16]. In [17], the capability of custom power devices, such as D-STATCOM and active filter is presented. Based on [17], this device can control the harmonic and reactive power of the nonlinear and linear loads. But, it is noted that the FACTS and custom power devices need high investment costs to be paid by one private company or distribution company. In addition, the bidirectional charger used in the technology of vehicle-to-X (V2X), and the concept of V2X, which transmits electricity from an on-board battery to the electrical infrastructure, is expected to be key solutions for the smart grids. With V2X technology, we can use electricity stored in the batteries of EVs and PHEVs when necessary [18]. Furthermore, different control strategies can be implemented for EV bidirectional charger to use them as an active filter and a D-STATCOM. For instance, the strategy of instantaneous active and reactive power (PQ) theory has been expressed in [19] and [20]. This method is adopted to create the reference current generation schemes related to harmonic, active and reactive power and unbalance compensation. In [21] and [22], the synchronous reference frame (SRF) theory is used for reference current generation in active filter and D-STATCOM related to harmonic, reactive power and unbalance compensation of nonlinear loads. Noted that different power decomposition theories are not suitable in the unity power factor operation, because there are some limitations on occurring resonance effects [23], [24]. Also, the frequency domain approaches such as fast Fourier transform (FFT), discrete Fourier transform (DFT) and recursive DFT lead to complex calculations, which in turn increase the computational burden [21]. However, in [25] and [26], the conservative power theory has been used for active filters. This method is the accurate current decomposition method and it has better features, such as accurate estimation under ideal and non-ideal grid voltages with selective estimation of disturbing effect [25], [26].

The main proposal of this paper is to activate the capabilities of the small-scale distributed resources in the system to improve power quality and network indexes. In other words, the EVs equipped with on-board bidirectional charger can control its battery power, reactive power, and harmonic current of nonlinear and linear loads. It is noted that the EVs' chargers can be installed on-board or off-board, where on-board charger is installed in the EV and off-board charger is installed in the electric vehicle supply equipment. Moreover, this paper assumes that the metering point is point of consumption rather than PCC. Therefore, the EV controls its active power based on the demand of its battery, and regulates its reactive power and harmonic current based on the demand of loads. Thus, it is expected to reduce the reactive power and harmonic current in the network side. Accordingly, by this scheme the total cost of power quality and network indexes improvement would be mainly paid by loads rather than network operators. Finally, this paper presents the suitable control strategy for bidirectional charger for providing the capability of power conditioning (including active and reactive power and harmonic current control). The proposed scheme is applied to the three-phase system that nonlinear and linear loads and EV are connected to the single phases. In the proposed strategy, both average and oscillatory components of the active and reactive powers are obtained using the three-phase instantaneous active and reactive power (PQ) theory. It is noteworthy that the main reason to use PQ theory is that this theory has a simple structure to be implemented with respect to the other control strategies. Thus, the applied active and reactive power to charger is calculated based on demand of EV and load. Finally, the reference current of ac/dc converter of charger and battery are obtained based on three-phase instantaneous PQ theory, and thus, the situation of charger switches are determined using proportional–integral (PI) and proportional–resonant (PR) controllers and pulsewidth modulation (PWM). Finally, the extensive studies and hardware-in-loop (HIL) simulations are presented, which prove the effectiveness of the proposed novel method. In summary, the main contributions of this paper are as follows:

1) using distributed resources for improvement of power quality and network indexes;

2) designing an on-board bidirectional charger for EVs to activate their capabilities in power conditioning.

The rest of the paper is organized as follows: Section II describes the proposed solution and system, and Section III

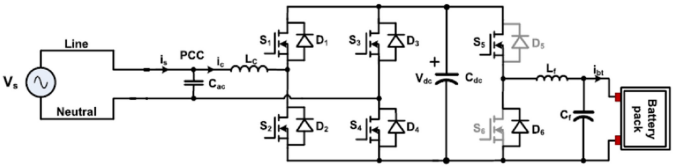

Fig. 1. Proposed structure of the on-board bidirectional charger [14].

expresses numerical simulations. Section IV demonstrates experimental results and conclusions, respectively.

II. Proposed Solution

As in many works in the area, the bidirectional structure for the ac/dc converter is used in this paper for power conditioning purposes of distribution networks, i.e., active and reactive power control and harmonic compensation of nonlinear loads. Accordingly, a specific control circuit design for this converter has been proposed.

A. Proposed Topology

It is noted that this paper presents the active and reactive power control as well as harmonic current control simultaneously using EV. Also, EV includes the battery and charger from the network's view point. The bidirectional charger is used as shown Fig. 1, in this paper, where it includes bidirectional ac/dc and dc/dc converters. Since the structure of the bidirectional AC/DC converter is like D-STATCOM, active filter or others FACTS, and custom power devices, therefore, this paper presents the active and reactive power control as well as harmonic current control simultaneously using EV. Also, the ac/dc converter is as full bridge converter that is comprised of a dc link capacitor, four transistors (MOSFETs or IGBTs), four diodes, and a coupling inductor as seen in Fig. 1. The topology is suitable for the proposed problem as done in [14] while it can provide low THD. Moreover, dc/dc converter is as half-bridge bidirectional converter in this paper, and it has two transistors (IGBT or MOSFET), two diodes, a filtering capacitor and an inductor as shown in Fig. 1. It can transfer power in both directions. Also, it can only operate as a buck converter in one direction and as boost converter in the opposite direction [14].

The framework of the proposed EV on-board bidirectional charger has been illustrated in Fig. 1. It is noted that the charger has a single-phase structure as shown in Fig. 1. However, to have a generic comprehensive model, the three-phase and four-wire system is considered for formulation as depicted in Fig. 2.

Accordingly, each phase includes one EV and a nonlinear/linear load, thus, the proposed system includes three EVs and loads. Also, the network and source are three-phase and four-wire systems. Indeed, presenting the proposed framework on the single-phase system is much more compatible to investigate the EVs' capabilities in the active and reactive power control and harmonic compensation of nonlinear loads. But, in this formwork, the sweeping model for the other studies, such as three-phase system balance, power system stability has not been presented yet. Hence, in the following sections, the sweeping

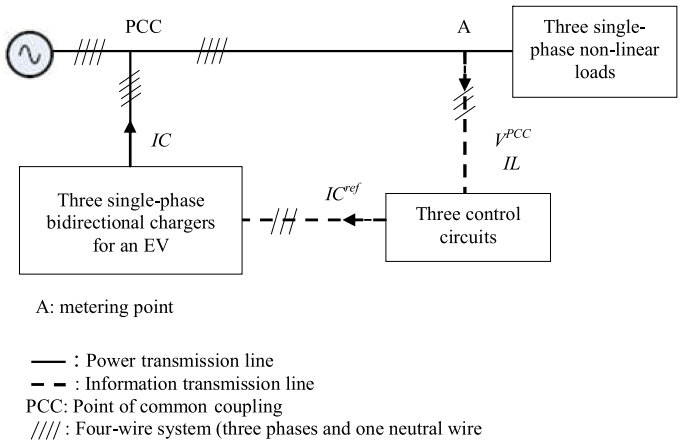

Fig. 2. Topology of proposed control scheme for EVs.

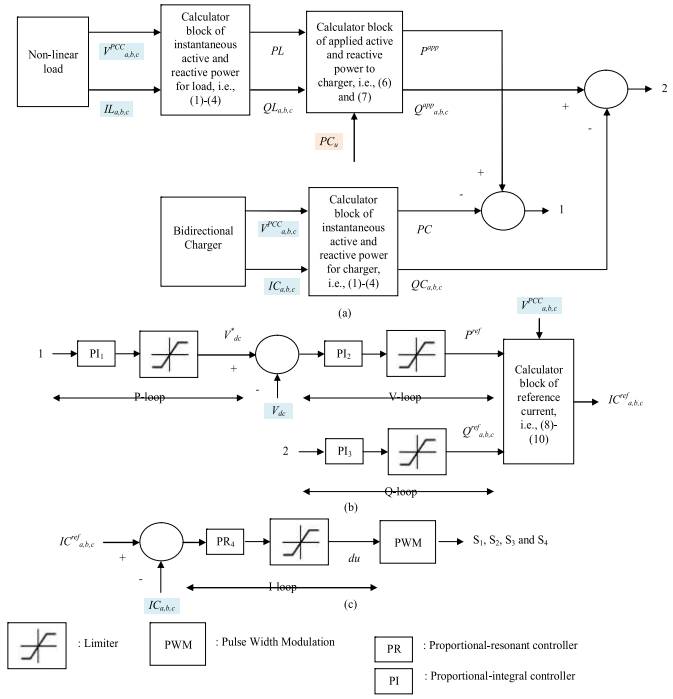

Fig. 3. Control circuit of the ac/dc converter. (a) Calculating the charger power. (b) Calculating reference current of the charger. (c) Determining the situation of ac–dc converter switches.

model on the three-phase and four-wire system is described. It should be noted that this paper investigates only the results of power conditioning (including active and reactive power control and harmonic control) or compensation for each individual EV. However, the model can be straightforwardly extended to consider a group of EVs.

B. Control Circuit for the Proposed System

Based on Fig. 1, the charger includes ac/dc and dc/dc converters, hence, this section presents the control of ac/dc and dc/dc converters as well.

1) Control Circuit of the ac/dc Converter: Fig. 3 shows the control circuit of the ac/dc converter. Based on this figure, the

proposed control model includes three groups of parameters as follows:

1) *Metering parameters*: These parameters are shown in Fig. 3 with blue colour, and these parameters are metered voltage and current at different points. Based on Figs. 2 and 3, the metering points in the location of load and charger or EV are used for metering of load and charger currents (*IL*, *IC*), respectively. Also, metering point of voltage (V^{PCC}) is PCC of network, load and charger.
2) *Decision parameters:* These parameters are shown in Fig. 3 with orange colour, and these parameters are determined using user preferences. For example, PC_u is specified based on decision of EV's owner.
3) *Calculated parameters:* These parameters are calculated based on metering and decision parameters and their corresponding relationships.

Based on Fig. 3, the control circuit of the ac/dc converter includes following blocks.

Calculator block of instantaneous active and reactive power: The calculator block of instantaneous active and reactive power is used for the calculation of load and charger instantaneous active and reactive power based on Fig. 3. Accordingly, the input of this block is metering parameters, such as PCC voltage and load (charger) current, and the output of this block is instantaneous active and reactive power of load or charge (EV). It is noted that active power is equal to dot (scalar) product (".") of voltage and current vectors, and reactive power is equal to cross product ("×") of voltage and current vectors [17]. In other words, if the voltage and current vectors are defined as (1) and (2), respectively, the instantaneous active and reactive power will be calculated based on (3) and (4), respectively [17]. Therefore, the active power is as scalar and reactive power is as vector. Noted that *IL* is used in the calculation of *PL* and *QL*, and *IC* is required to determine the *PC* and *QC* in (3) and (4).

$$V^{\mathrm{PCC}} = \begin{bmatrix} V_a^{\mathrm{PCC}} & V_b^{\mathrm{PCC}} & V_c^{\mathrm{PCC}} \end{bmatrix} \tag{1}$$

$$I = \begin{bmatrix} I_a & I_b & I_c \end{bmatrix} \quad \forall I \in \{IL, IC\} \tag{2}$$

$$P = V^{\mathrm{PCC}}.I = V_a^{\mathrm{PCC}} I_a + V_b^{\mathrm{PCC}} I_b + V_c^{\mathrm{PCC}} I_c \quad \forall I \in \{IL, IC\}, P \in \{PL, PC\} \tag{3}$$

$$Q = V^{\mathrm{PCC}} \times I = \begin{bmatrix} Q_a \\ Q_b \\ Q_c \end{bmatrix} = \begin{bmatrix} \begin{vmatrix} V_b^{\mathrm{PCC}} & V_c^{\mathrm{PCC}} \\ I_b & I_c \end{vmatrix} \\ \begin{vmatrix} V_c^{\mathrm{PCC}} & V_a^{\mathrm{PCC}} \\ I_c & I_a \end{vmatrix} \\ \begin{vmatrix} V_a^{\mathrm{PCC}} & V_b^{\mathrm{PCC}} \\ I_a & I_b \end{vmatrix} \end{bmatrix} \quad \forall I \in \{IL, IC\}, Q \in \{QL, QC\}. \tag{4}$$

It is noted that the (1) to (4) are based on three-phase instantaneous active and reactive power (PQ) theory [17]. However, if the proposed system has as single-phase, hence, it needs to implement single-phase instantaneous active and reactive power theory as presented in [27] and [28]. Accordingly, the proposed system can be changed to single-phase system, while the calculator block of the instantaneous active and reactive power is based on single-phase instantaneous PQ theory. In addition, the scalar value of reactive power is needed in some cases, and it is obtained as follows [17]:

$$Q = \frac{Q_a + Q_b + Q_c}{\sqrt{3}} \quad Q \in \{QL, QC\}. \tag{5}$$

Based on [17], the power is equal to summation of average power (P_{avg}, Q_{avg}) and oscillatory power (P_{osc}, Q_{osc}). The average power obtained based on the symmetrical (positive sequence) and fundamental frequency component of voltage and current, and the oscillatory power is equal to summation of power due to harmonic frequency components (P_h, Q_h) and power due to unbalance system (negative and zero sequences) that is shown as $P_{2\omega}$ and $Q_{2\omega}$, and its frequency is equal to 200% of the fundamental frequency of the network (ω) [17].

Calculator block of applied active and reactive power to charger: The calculator block of the applied active and reactive power to charger is used for calculation of the applied active and reactive power to charger based on Fig. 3. Based on Fig. 3, the input of this block is the active and reactive power of the load (*PL*, *QL*) and required active power of battery from the network viewpoint that is demanded by EV user (PC_u). Noted that the charger active power (PC_u) is equal to the summation of the battery active power and charger active loss. The output of this block is applied active and reactive power of the charger (P^{app}, Q^{app}) that includes oscillatory active power of load (PL_h, $PL_{2\omega}$) and oscillatory (QL_h, $QL_{2\omega}$) and average (QL_{avg}) reactive power of load (these terms are removed using charger), and required active power of battery from the network side. Therefore, the relationship between input and output of this block is as (6) and (7) for active and reactive terms, respectively,

$$P^{\mathrm{app}} = a_1 PL_{\mathrm{avg}} + a_2 PL_h + a_3 PL_{2\omega} + a_4 PC_u \tag{6}$$

$$Q^{\mathrm{app}}_{a,b,c} = b_1 QL_{\mathrm{avg}_{a,b,c}} + b_2 QL_{h_{a,b,c}} + b_3 QL_{2\omega_{a,b,c}}. \tag{7}$$

In these equations, the coefficients of a_i and b_i are decision making parameters that are one or zero. But, coefficient of a_4 is equal to –1 while EV battery is in the discharging mode. It is noted that these parameters are determined based on the preferences of users. Moreover, PL_{avg} and QL_{avg} (PL_h and QL_h) can be obtained using low-pass filter (high-pass filter) with low set-frequency (set-frequency is more than network frequency, i.e., 50 or 60 Hz), where this filter is located after *PL* and *QL*, respectively. But, $PL_{2\omega}$ and $QL_{2\omega}$ are obtained using band-pass filter with the set-frequency of 100 to 120 Hz [14]. In addition, the limits of the proposed charger are capacity and battery charge/discharge rate limits which expressed as $(P^{\mathrm{app}})^2 + (Q^{\mathrm{app}})^2 \leq (SC)^2$ and $DR \leq PC_u \leq CR$, respectively. *SC* is charger capacity, and *CR* and *DR* are the battery charging and discharging rates, respectively, [10]. In addition, Q^{app} is provided by the charger and it is not dependent of battery. But, P^{app} depends on active load and the required active power of battery from the network (PC_u). Note, PL_{avg} is provided by the network, and PL_h and $PL_{2\omega}$ are provided by battery in harmonic comparison mode. But, the values of PL_h and $PL_{2\omega}$ are

more less than $PL_{\rm avg}$. Moreover, PC_u makes the state of charge (SOC) or depth of discharge (DOD), because it is sent to battery from the network, or vice versa. Thus, this power changes the stored energy in battery, changing this energy causes changing of SOC or DOD. Since, this control action takes place in about 10 s, therefore, the SOC or DOD is almost constant. In other words, if the simulation times were about some hours, thus, the SOC and DOD would be changed during the control process as we studied it in our previous work [10]. Finally, it is noted that the models of the battery and EV's charger have been considered in this paper.

Calculator block of reference current: The calculator block of reference current is used for calculation of charger reference current. Based on Fig. 3, the input of this block is the reference active and reactive power of the charger, and the output of this block is the charger reference current. The proposed system as Fig. 2 is based on three-phase instantaneous PQ theory, hence, the calculator block of reference current is based on this theory. According to this theory [17], the reference current includes active (IC^p) and reactive (IC^q) components as (8), and these components are due to the active and reactive powers as (9) and (10), respectively,

$$IC^{\rm ref}_{a,b,c} = IC^{p}_{a,b,c} + IC^{q}_{a,b,c} \tag{8}$$

$$IC^{p} = \frac{P^{\rm ref}}{V^{\rm PCC}.V^{\rm PCC}} V^{\rm PCC} = \begin{bmatrix} IC^p_a & IC^p_b & IC^p_c \end{bmatrix}^T = \frac{P^{\rm ref}}{(V^{\rm PCC}_a)^2 + \left(V^{\rm PCC}_b\right)^2 + (V^{\rm PCC}_c)^2} \begin{bmatrix} V^{\rm PCC}_a & V^{\rm PCC}_b & V^{\rm PCC}_c \end{bmatrix}^T \tag{9}$$

$$IC^{q} = \frac{Q^{\rm ref} \times V^{\rm PCC}}{V^{PCC}.V^{\rm PCC}} = \begin{bmatrix} IC^q_a & IC^q_b & IC^q_c \end{bmatrix}^T = \frac{1}{(V^{\rm PCC}_a)^2 + \left(V^{\rm PCC}_b\right)^2 + (V^{\rm PCC}_c)^2} \begin{bmatrix} \begin{vmatrix} Q^{\rm ref}_b & Q^{\rm ref}_c \\ V^{\rm PCC}_b & V^{\rm PCC}_c \end{vmatrix} \\ \begin{vmatrix} Q^{\rm ref}_c & Q^{\rm ref}_a \\ V^{\rm PCC}_c & V^{\rm PCC}_a \end{vmatrix} \\ \begin{vmatrix} Q^{\rm ref}_a & Q^{\rm ref}_b \\ V^{\rm PCC}_a & V^{\rm PCC}_b \end{vmatrix} \end{bmatrix}. \tag{10}$$

Equation (1)–(10) are obtained based on PQ theory, therefore, these equations should be changed in the other control methods based on the corresponding theory.

It is noted that the reference active and reactive power ($P^{\rm ref}$, $Q^{\rm ref}$) obtained with following formulations using suitable controller based on Fig. 3. Based on this figure, there are outer and inner loops for active power control, that the outer loop is used to satisfy active power condition (active power of charger output should be equal to applied active power to the charger) by modifying the set-point of dc-link voltage ($V^*_{\rm dc}$). Also, this loop is called active power loop that is shown as *P*-loop, and it includes PI controller as follows:

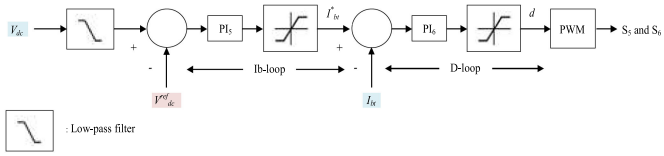

Fig. 4. Control block diagram of the dc/dc converter.

$$V^*_{\rm dc} = K^P_{P-{\rm loop}} \left(P^{\rm app} - PC\right) + \frac{K^I_{P-{\rm loop}}}{s} \left(P^{\rm app} - PC\right). \tag{11}$$

The inner loop or dc voltage loop (*V*-loop) is used to follow $V^*_{\rm dc}$, i.e., the voltage of dc-link should be equaled to $V^*_{\rm dc}$. This loop uses PI controller that its output is reference active power as

$$P^{\rm ref} = K^P_{V-{\rm loop}} \left(V^*_{\rm dc} - V_{\rm dc}\right) + \frac{K^I_{V-{\rm loop}}}{s} \left(V^*_{\rm dc} - V_{\rm dc}\right). \tag{12}$$

Moreover, the reactive power control includes outer loop that is shown as *Q*-loop. This loop includes PI controller and it is used to satisfy reactive power condition (reactive power of charger output should be equal to the applied reactive power to charger) by modifying the reference reactive power as

$$Q^{\rm ref}_{a,b,c} = \left(K^P_{Q-{\rm loop}} + \frac{K^I_{Q-{\rm loop}}}{s}\right). \left(Q^{\rm app}_{a,b,c} - QC_{a,b,c}\right). \tag{13}$$

Finally, the situation of the ac/dc converter switches is determined using PWM. The input of PWM is current loop (*I*-loop) that is used to follow $IC^{\rm ref}$, i.e., the current of the charger output should be equal to $IC^{\rm ref}$. It is noted that this loop uses the PR controller [29] that its output is applied signal to PWM (*du*) as

$$du_{a,b,c} = \left(K^P_{I-{\rm loop}} + \frac{2K^I_{I-{\rm loop}}\omega_c s}{s^2 + 2\omega_c s + (\omega)^2}\right). \left(IC^{\rm ref}_{a,b,c} - IC_{a,b,c}\right). \tag{14}$$

2) Control Circuit of the dc/dc Converter: Fig. 4 shows the control circuit of the dc/dc converter. Based on this figure, there are outer and inner loops for active power control, that the outer loop (Ib-loop) is used to satisfy dc voltage condition (voltage of dc-link should be equal to reference dc-link voltage or $V^{\rm ref}_{\rm dc}$) by modifying the reference battery current (I^*_{bt}).

Also, this loop uses the PI controller as shown in (15), and it is used as a complement for the *P*-loop that its purpose is the establishment of balance between active power of the charger output and the applied active power to the charger.

$$I^*_{bt} = K^P_{Ib-{\rm loop}} \left(V_{\rm dc} - V^{\rm ref}_{\rm dc}\right) + \frac{K^I_{Ib-{\rm loop}}}{s} \left(V_{\rm dc} - V^{\rm ref}_{\rm dc}\right). \tag{15}$$

Regarding the voltage of the dc-link, $V_{\rm dc}$, it depends on $P^{\rm app}$ and the current of battery. Thus, $V_{\rm dc}$ will be close to $V^{\rm ref}_{\rm dc}$ (it is 400 V in this paper) by $\rm PI_5$ controller or (15) based on Fig. 4.

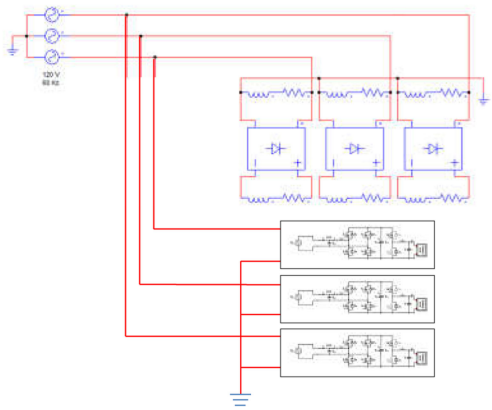

Fig. 5. Proposed circuit for the simulations.

Also, dc-link voltage that is related to P^{app} or P^{ref} (V_{dc}^{*}) is extracted by PI_1 controller or (11), and it should be close to V_{dc} based on PI_2 controller or (12). Finally, based on (11), (12), and (15), V_{dc}^{*} should track $V_{\text{dc}}^{\text{ref}}$, therefore, with this method, V_{dc} is controlled to track the set-point $V_{\text{dc}}^{\text{ref}}$. In other words, the proposed system in Fig. 2 uses the dc-link voltage control to generate battery reference current (I_{bt}^{*}) in the dc/dc converter. Note that if P^{app} increases/decreases, then, V_{dc} is increased/decreased to a new set-point based on the (11) and (12). This small increases/decreases in V_{dc} yields an increase/decrease in the battery current (I_{bt}).

It is important to note that initial SOC and battery size of the EV do not affect the proposed strategy performance. In other words, the SOC is equal to the stored energy (E)/battery capacity. The stored energy is expressed as $E_t = E_{t-1} + \Delta t \times \eta PC_u$, where η is charger round-trip efficiency and PC_u is the active power of battery or the charger. Thus, based on this equation, the SOC or DOD depends to time (Δt) such as 1 h. However, in this paper, the simulation is run for 10 s. That is, the value of SOC is constant in this period of simulation. Thus, the changing of SOC or DOD is about zero. Also, the charge/discharge rates of the battery are considered in this paper, and they depend on PC_u, where PC_u has been explained in (6). The inner loop (D-loop) calculates duty cycle of the dc/dc converter based on the error between reference and metering battery current using PI controlled and with (16). Finally, the duty cycle of the dc/dc converter is applied to PWM for determination of the situation of ac/dc converter switches.

$$d = K_{D-\text{loop}}^{P}\left(I_{bt}^{*} - I_{bt}\right) + \frac{K_{D-\text{loop}}^{I}}{s}\left(I_{bt}^{*} - I_{bt}\right). \tag{16}$$

III. Numerical and Experimental Results and Discussion

A. Case Study

To evaluate the capability of the proposed system with the simulation circuit in Fig. 5, the HIL simulation approach has been used. The real-time HIL method is used to emulate errors and delays that do not exist in the classical offline simulations. Fig. 6 illustrates the HIL setup consisting of OPAL-RT as a real-time simulator, which simulates the suggested circuit presented in Fig. 5, a PC as the command station (programming host) in which the MATLAB/Simulink-based code will be executed on the OPAL-RT, and a router that is used as a connector of all the setup devices in the same sub-network. The OPAL-RT is also connected to DK60 board through Ethernet ports. More details about this setup can be found in [30] and [31]. In other words, this method includes simulation and hardware parts, where Fig. 5 is in the simulation part and different controls are in the hardware part. Based on [30] and [31], the error of this method with respect to experimental platform is very low and accordingly this approach has been adopted in many research works in the area.

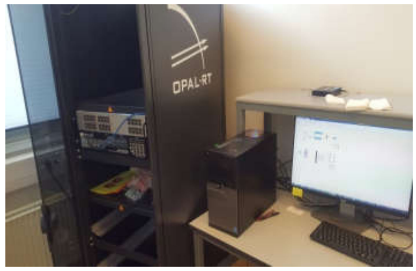

Fig. 6. Real-time experimental setup.

TABLE I
Characteristics of the Bidirectional Charger [14]

Parameter	Symbol	Value
Capacity	*SC*	1.44 kVA
Battery charge/discharge rate	*CR/DR*	1000/-1000 W
Supply voltage	*VC*	120 V
Maximum current	*IC*	12 A
Coupling inductance	L_c	1 mH
Switching frequency of AC/DC converter	$f_{sw1\text{-}4}$	10 kHz
DC-link voltage	V_{dc}	400 V
DC-link capacitor	C_{dc}	330 μF
Switching frequency of DC/DC converter	$f_{sw5\text{-}6}$	10 kHz
Battery side filter capacitor	C_f	200 μF
Battery side filter inductance	L_f	400 μH

This simulation includes linear and nonlinear loads. The linear load is as series circuit of resistance-inductance and the value of resistance and inductance is 8.7 Ω and 20 mH, respectively. Also, the nonlinear load is as a single-phase rectifier with series circuit of resistance–inductance in the output of single-phase rectifier, which the value of resistance and inductance is 8.7 Ω and 20 mH, respectively. The network voltage and frequency is 120 V and 60 Hz, respectively. Tables I and II present the bidirectional charger characteristics, and the PI/PR controller characteristics [14].

Also, the decision making coefficients of a_3 and b_3 are considered to be zero, because this paper investigates the EV capability for the active and reactive power control and harmonic compensation of nonlinear load, that is, the system unbalance mode is not considered. Finally, the battery model has been presented in [32].

B. Method

In this paper, the HIL simulation approach is used to obtain the proposed system results and investigate the capability of the EV charger. Also, the real-time HIL method is used to emulate errors and delays that do not exist in the classical offline simulations.

TABLE II
CHARACTERISTICS OF PI AND PR CONTROLLERS [14]

Controller		Parameter	Value
PI_1	P-loop	K^P	1
		K^I	20
PI_2	V-loop	K^P	1.5
		K^I	100
PI_3	Q-loop	K^P	0.1
		K^I	30
PR_4	I-loop	K^P	0.6
		K^I	500
		ω_c	3 rad/s
PI_5	Ib-loop	K^P	0.045
		K^I	0.5
PI_6	D-loop	K^P	0.01
		K^I	10

1) Investigating Charger Operating Areas in the Average Power Control Condition: In this section, the simulation results of the average active and reactive power control are expressed. Hence, the decision making coefficients of a_2, a_3, b_2, and b_3 are equal to zero. Also, the different cases have been investigated as follows.

Case I: Investigating of simulation results in EVs are operated in the capacitive and charging modes.
Case II: EVs are operated in the inductive and charging modes.
Case III: EVs are operated in the capacitive and discharging modes.
Case IV: EVs are operated in the inductive and discharging modes.

The results of this section have been presented in Fig. 7. Accordingly, the average active and reactive loads are equal to 7000 W and 3250 var in the steady-state condition. In the cases of I–IV, the charging/discharging active power is considered to be 850 W for each EV, and the total average reactive power of EVs is equal to the total average reactive power of loads (3250 var). Hence, in the steady–state condition and based on Fig. 7, the average active power of EVs is 2550 W in the cases I and II, and it is –2550 W in the cases III and IV. It is noted that the average active power of EVs shows the battery operation, i.e., if the average active power of EVs is positive (negative), thus, the EV's battery operates in the charging (discharging) mode. Moreover, the average active power of the network is 9550 and 4450 W for cases I and II, and cases III and IV, respectively. In other words, the average active power of the network increases about 36.5% for cases I and II, and it reduces about 36.5% for cases III and IV with respect to the results of the load active power. It is noted that in the cases I and III, the EV charger operates in the capacitive mode. Hence, based on Fig. 7, the average reactive power of EVs is equal to –3250 var, and the average reactive power of the network is equal to zero in the steady-state condition. Therefore, the EVs charger compensates all average reactive power of the loads. But, the EV charger acts in inductive mode for cases II and IV, hence, the average reactive power of EVs and network is equal to 3250 and 6500 var based on Fig. 7, respectively. Therefore, the average reactive power of the network increases about 100% with respect to the load reactive power.

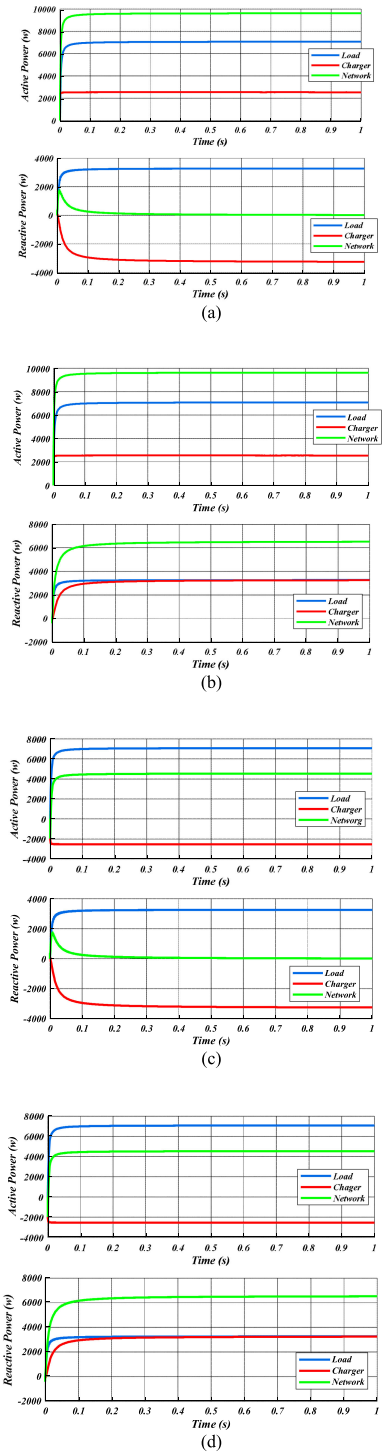

Fig. 7. Average active and reactive power for different parts of the proposed system. (a) Case I. (b) Case II. (c) Case III. (d) Case IV.

Also, the time constant of charger active power is less than other parameters, such as the network and load power and charger reactive power. Because, the number of calculator blocks is low for the calculation of the charger active power, but the number of calculator blocks is high for the calculation of other parameters.

Based on Fig. 7, the EV charger can act as a power customer or power producer with suitable control of its switches. This

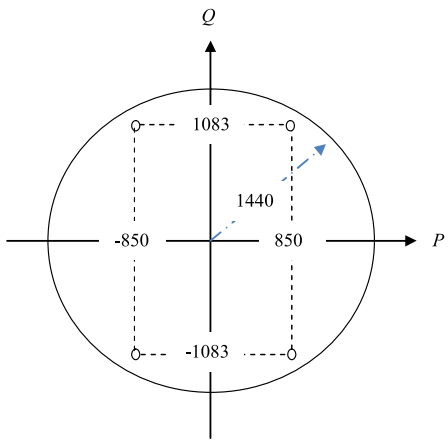

Fig. 8. Operating area of an EV in the *PQ* plane.

statement has been illustrated in Fig. 8 for one EV charger. According to this figure, the EV charger can be operated in all areas of *PQ* plane. It should be noted that the different values in Fig. 8 are obtained from the results of Fig. 7. Hence, EV can operate as capacitive, inductive, and resistive loads or a complex of them based on the right side of the operating areas in *PQ* plane of Fig. 8. In contrast, it can act as active power supply, reactive power supply, inductive load or complex of them based on the left side of operating areas in *PQ* plane of Fig. 8. Moreover, the operating area of the EV charger is equal to inner areas and the border of circle with radius that is equal to charger capacity (1440 VA for proposed system).

2) Investigating Harmonic Compensation Using EVs: In this section, the simulation results for the harmonic compensation of the nonlinear load using EV bidirectional charger have been presented. Accordingly, the coefficients of a_3, and b_3 are equal to zero. Also, the following cases have been studied.

Case I: Investigating the proposed system without considering EVs.

Case II: Investigating the proposed system considering EVs that are operating as harmonic compensators in the capacitive and charging modes.

Case III: Investigating the proposed system considering EVs that are operating as harmonic compensators in the capacitive and discharging modes.

Fig. 9 shows the results of this section. As seen, the load current wave is not sinusoidal due to the presence of single-phase rectifier in the consumption side. Moreover, the load current magnitude for the harmonic orders 3, 5, and 7 is equal to 4, 2.5, and 1.8 A, that these values are high with respect to the load current magnitude at the fundamental frequency, i.e., 31 A. Because, the maximum current magnitudes are equal to 4%, 2%, 1.5%, 0.6%, and 0.3% of current magnitudes at the fundamental frequency for $h < 11$, $11 \leq h < 17$, $17 \leq h < 23$, $23 \leq h < 35$ and $h \geq 35$, respectively, based on standard of IEEE STD. P519.1/D9A [33], and h is the harmonic order. Also, in cases II and III, the charging/discharging active power is considered to 800 W for each EV, and the total average reactive power of EVs is equal to 3250 var. Finally, it is considered that the EVs can compensate all harmonics of the nonlinear loads. Based on

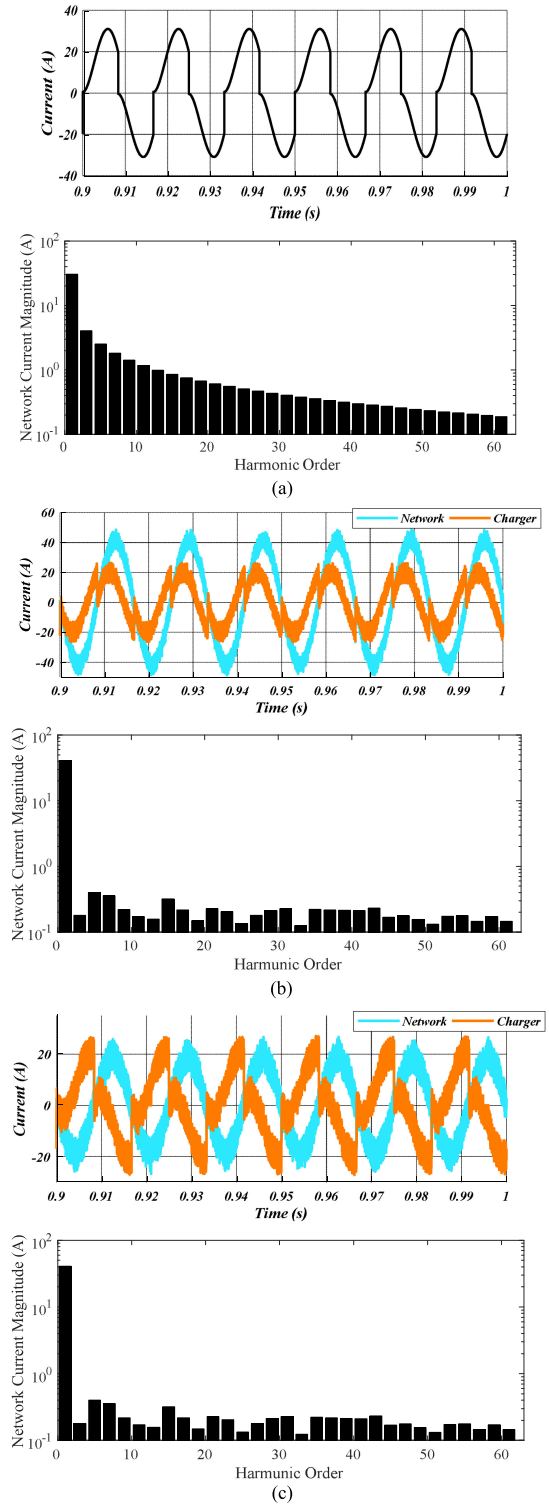

Fig. 9. Current and harmonic current for different parts of the network. (a) Case I. (b) Case II. (c) Case III.

Fig. 9, the average network current wave is as sinusoidal wave, but the average EV current wave is not as the sinusoidal wave in cases II and III. Because, the harmonic of the load side is compensated by EVs in these cases. It is noted that the network and EV currents include ripples mounted on the sinusoidal or nonsinusoidal waves due to switching of the charger switches. However, the magnitude of ripple can be reduced using suitable

TABLE III
NETWORK CURRENT THD, DC-LINK VOLTAGE, AND BATTERY CURRENT

Case	Network current THD (%)	DC-link voltage (V)		Battery current (A)	
		Value	Ripple	Value	Ripple
I	19.64	-	-	-	-
II	7.42	400	3	6.3	0.3
III	8.54	400	3	-7	0.35

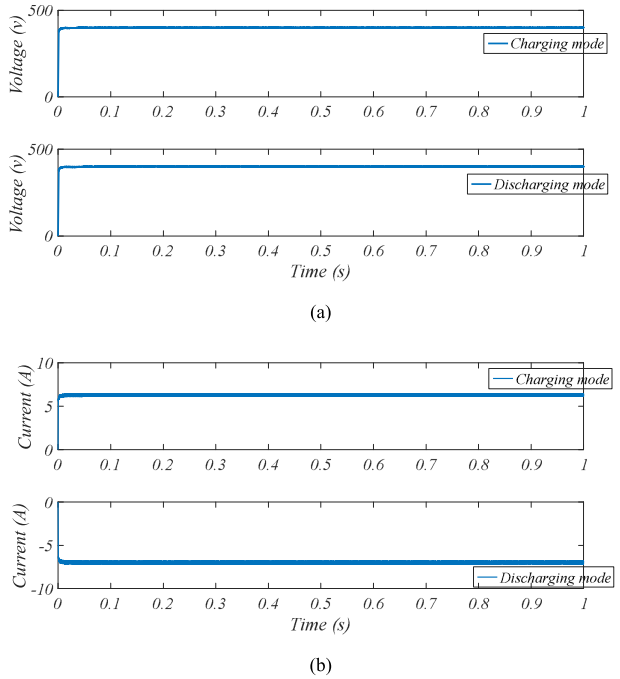

Fig. 10. DC side results in Cases II and III. (a) DC-link voltage. (b) Battery current.

regulation of PI and PR controller parameters and inductance of L_c. In addition, the network current magnitude is reduced in harmonic frequency components with respect to the case I. Also, the harmonic current magnitudes of the network satisfy IEEE STD. P519.1/D9A [33].

Table III presents the THD of the network current, dc-link voltage ($V_{\rm dc}$) and battery current for cases I–III. Based on the table, the network current THD is equal to 20% in case I, thus, it is high based on the standard of IEEE STD. P519.1/D9A. But, it is reduced about 57% in cases II and III with respect to the case I, and it satisfies the standard condition of IEEE STD. P519.1/D9A.

Moreover, the dc-link voltage is equal to 400 V for cases II and III in the steady-state condition based on Fig. 10(a). Also, the time constant is much small for dc-link voltage according to this figure. As seen in Table III and Fig. 10(b), the battery current is equal to 6.3 and –7 A for charging and discharging modes. Noted that if each EV injects or absorbs only 800 W to/from network, therefore, the current magnitude between network and charger is 6.66 A (800 W/120 V). However, due to the power loss of ac/dc and dc/dc converters provided by the battery, the battery current magnitude has been increased in the discharging mode with respect to 6.66 A. In addition, it is reduced in the charging mode with respect to 6.66 owing to the power loss of ac/dc and dc/dc converters provided by the network. Moreover, the battery current shows the battery operation, i.e., if the battery current is positive (negative), then, the EV's battery operates in the charging (discharging) mode. Finally, it is seen that the time constant is very small for the battery current based on Fig. 10(b).

TABLE IV
COMPARISON BETWEEN DIFFERENT CONTROL STRATEGIES

Case II (EV is as harmonic compensator in the capacitive/charging modes)						
Method	Network current		DC-link voltage (V)		Battery current (A)	
	RMS (A)	THD (%)	Value	Ripple	Value	Ripple
Proposed strategy	28.4	7.42	400	3	6.3	0.3
SRF [22]	28.4	7.88	400	3.4	6.3	0.4
FFT [21]	28.4	7.57	400	3.6	6.3	0.45
Case III (EV is as harmonic compensator in the capacitive/discharging modes)						
Method	Network current		DC-link voltage (V)		Battery current (A)	
	RMS (A)	THD (%)	Value	Ripple	Value	Ripple
Proposed strategy	13.8	8.54	400	3	-7	0.35
SRF [22]	13.8	8.68	400	3.45	-7	0.45
FFT [21]	13.8	8.62	400	3.7	-7	0.55

3) Comparison of Results Between Different Control Strategies: Table IV presents the results of this section including the network current THD and RMS, dc-link voltage and battery current with different control strategies based on PQ theory, SRF theory [22], and FFT [21] for cases II and III in the previous Section III-B-2. Also, it is noted that the all parameters of the proposed system are the same for all control strategies. The results in this table have been presented for three main parts as follows.

1) Network current RMS and THD show the characterizes of the network or voltage source in Fig. 5, where as seen in the table, the network current RMS is the same for different control strategies while there are the same characteristics in Fig. 5 and the same demand from the network by EVs and loads for all control strategies. Also, the network current RMS in the case II is more than case III, because the EVs receive the active power from the network in the case II, while they inject the active power into the network at the case III. In addition, the network current THD in the proposed control strategy (PQ theory) is suitable with respect to the SRF and FFT methods for cases II and III.
2) In the dc-link part, the value and ripple of the dc-link voltage have been presented in Table IV. Indeed, the value of the dc-link voltage is the same for all control strategies and cases and it is equal to 400 V, because the voltage of the dc-link should follow the reference voltage (400 V based on Table I) according to (11), (12), and (15). In addition, the ripple of voltage in the DC-link for the proposed control strategy is low in comparison with the other control strategies.
3) In the battery side, the value and ripple of battery current have been addressed in Table IV. The battery current value is the same in all control strategies since there is the same active power (charging in case II and discharging in case

III) in battery side for all strategies. Also, the ripple of the battery current is low in the proposed method with respect to the SRF and FFT.

Finally, based on the results of this table, the proposed control strategy (PQ theory) has suitable results for different parameters as shown in Table IV with respect to the SRF and FFT methods.

IV. Conclusion

This paper designs an on-board bidirectional charger for a single-phase EV with the capability of power conditioning (including active and reactive power as well as harmonic current control). It is assumed that the general three-phase system includes some single-phase nonlinear and linear loads and EVs. Accordingly, the proposed control strategy is based on the three-phase instantaneous PQ theory wherein the power (active and reactive) includes both average and oscillatory components. The average power is obtained based on the fundamental frequency and the positive sequence of the voltage and current signals, while the oscillatory power is obtained based on the harmonic frequency and the negative and zero sequences of voltage and current signals. Consequently, the situation of charger switches are determined using the PI and PR controllers combined with PWM. Based on the numerical and experimental results, the EV bidirectional charger can operate in four quadrants in the active-reactive (PQ) power plane, and it can compensate for the nonlinear harmonic currents.

To have a further exploration in this area, the research work is underway to model the EVs in the context of the optimal harmonic power flow using new control strategy for the proposed charger and implement it in real cases.

References

[1] S. Shafiee *et al.*, "Investigating the impacts of plug-in hybrid electric vehicles on power distribution systems," *IEEE Trans. Smart Grid.*, vol. 4, no. 3, pp. 1351–1360, Sep. 2013.

[2] R. C. Leou, C. L. Su, and C. N. Lu, "Stochastic analyses of electric vehicle charging impacts on distribution network," *IEEE Trans. Power Syst.*, vol. 29, no. 3, pp. 1055–1063, May 2013.

[3] S. Rezaee, E. Farjah, and B. Khorramdel, "Probabilistic analysis of PHEVs impact on electrical grid through homes and parking lots," *IEEE Trans. Sustain. Energy*, vol. 4, no. 4, pp. 1024–1033, 2013.

[4] J. C. Gomez and M. M. Morcos, "Impact of EV battery chargers on the power quality of distribution system," *IEEE Trans. Power Del.*, vol. 22, no. 10, pp. 975–981, Oct. 2003.

[5] L. Kutt, E. Saarijarvi, M. Lehtonen, H. Molder, and J. Niitsoo, "A review of the harmonic and unbalance effects in electrical distribution networks due to EV charging," in *Proc. Int. Conf. Environ. Elect. Eng.*, 2013, pp. 556–561.

[6] M. Kuss, T. Markel, and W. Karmer, "Application of distribution transformer thermal life models to electrified vehicle charging load using monte-carlo method," in *Proc. Elect. Vehicle Symp., Shenzen*, 2010, pp. 5–9.

[7] R. Godina, E. M. G. Rodrigues, J. C. O. Matias, and J. P. S. Catalão, "Smart electric vehicle charging scheduler for overloading prevention of an industry client power distribution transformer," *Appl. Energy*, vol. 178, pp. 29–42, 2016.

[8] C. Jiang, R. Torquato, D. Salles, and W. Xu, "Method to assess the power quality impact of plug- in hybrid electric vehicles," *IEEE Trans. Power Del.*, vol. 29, no. 4, pp. 958–965, Apr. 2014.

[9] S. Pirouzi, M. A. Latify, and G. R. Yousefi, "Investigation on reactive power support capability of PEVs in distribution network operation," in *Proc. 23rd Iranian Conf. Elect. Eng.*, May 2015, pp. 1591–1596.

[10] S. Pirouzi, J. Aghaei, M. A. Latify, G. R. Yousefi, and G. Mokryani, "A robust optimization approach for active and reactive power management in smart distribution networks using electric vehicles," *IEEE Syst. J.*, vol. 12, no. 3, pp. 2699–2710, Sep. 2017.

[11] L. Yanxia and J. Jiuchun, "Harmonic-study of electric vehicle chargers," in *Proc. 8th Int. Conf. Elect. Mach. Syst.*, Sep. 2005, pp. 2404–2407.

[12] T. Tanaka, T. Sekiya, H. Tanaka, M. Okamoto, and E. Hiraki, "Smart charger for electric vehicles with power-quality compensator on single-phase three-wire distribution feeders," *IEEE Trans. Ind. Appl.*, vol. 49, no. 6, pp. 2628–2635, Nov./Dec. 2013.

[13] M. Kesler, M. C. Kisacikoglu, and L. M. Tolbert, "Vehicle-to-grid reactive power operation using plug-in electric vehicle bidirectional offboard charger," *IEEE Trans. Ind. Electron.*, vol. 61, no. 12, pp. 6778–6784, Dec. 2014.

[14] M. C. Kisacikoglu, M. Kesler, and L. M. Tolbert, "Single-phase on-board bidirectional PEV charger for V2G reactive power operation," *IEEE Trans. Smart Grid*, vol. 6, no. 2 pp. 767–775, Mar. 2015.

[15] M. R. Asban, J. Aghaei, T. Niknam, and M. A. Akbari, "Designing static var compensator capacity to enhance power quality in electric arc furnaces," *Trans. Soc. Model. Simul. Int.*, vol. 93, no. 5, pp. 515–525, 2017.

[16] N. G. Hingorani and L. Gyugyi, *Understanding FACTS*. New York, NY, USA: IEEE Press, 1999.

[17] A. Ghosh and G. Ledwich, *Power Quality Enhancement Using Custom Power Devices*. Norwell, MA, USA: Kluwer, 2002.

[18] T. Izumi *et al.*, "Bidirectional charging unit for vehicle-to-X (V2X)," *Sei Techn. Rev.*, pp. 39–42, 2014.

[19] F. Z. Peng and J. S. Lai, "Generalized instantaneous reactive power theory for three-phase power systems," *IEEE Trans. Instrum. Meas.*, vol. 45, no. 1, pp. 293–297, Feb. 1996.

[20] H. Akagi, E. H. Watanabe, and M. Aredes, *Instantaneous Power Theory and Applications for Power Conditioning*. Hoboken, NJ, USA: Wiley, 2007, pp. 41–102, 2007.

[21] L. Asiminoaei, F. Blaabjerg, and S. Hansen, "Detection is key-harmonic detection methods for active power filter applications," *IEEE Ind. Appl. Mag.*, vol. 13, no. 4, pp. 22–33, Jul./Aug. 2007.

[22] M. Maciążek, *Power Theories Applications to Control Active Compensators*. London, U.K.: Springer, 2012 pp. 49–116.

[23] M. E. Balci and M. H. Hocaoglu, "A power resolution for nonsinusoidal and unbalanced systems – part II: Theoretical background," in *Proc. 17th IEEE Int Conf. Elect. Electron. Eng.*, 2011, pp. I-173–I-178.

[24] M. E. Balci and M. H. Hocaoglu, "Addendum to a power resolution for nonsinusoidal and unbalanced systems: Evaluation examples," in *Proc. 17th IEEE Int. Conf. Elect. Electron. Eng.*, 2011, pp. I-179–I-182.

[25] A. Mortezaei, C. Lute, and M. Godoy Simões, "PQ, DQ, and CPT control methods for shunt active compensators—a comparative study," in *Proc. IEEE Energy Convers. Congr. Expo.*, Pittsburgh, PA, USA, 2014, pp. 2994–3001.

[26] V. S. R. V. Oruganti, A. S. Bubshait, V. S. S. S. S. Dhanikonda, and M. G. Simões, "Real-time control of hybrid active power filter using conservative power theory in industrial power system," *IET Power Electron.*, vol. 10, no. 2, pp. 196–207, 2017.

[27] H. Akagi *et al.*, "Instantaneous reactive power compensators comprising switching devices without energy storage elements," *IEEE Trans. Ind. Appl.*, vol. 20, no. 3, pp. 625–630, Mar. 1984.

[28] A. H. Ukande, S. L. Tiwari, S. G. Kadwane, and A. Kadu, "Generalise PQ theory with SPWM for single phase shunt active filter applications," in *Proc. IEEE Power, Commun. Inf. Technol. Conf.*, 2015, pp. 1–6.

[29] R. Teodorescu *et al.*, "Proportional-resonant controllers and filters for grid-connected voltage-source converters," *IEE Proc. Elect. Power Appl.*, vol. 153, no. 5, pp. 750–762, Sep. 2006.

[30] M. Rakhshan, N. Vafamand, M. H. Khooban, and F. Blaabjerg, "Maximum power point tracking control of photovoltaic systems: A polynomial fuzzy model-based approach," *IEEE J. Emerg. Sel. Topics Power Electron.*, vol. 6, no. 1, pp. 292–299, Mar. 2018.

[31] Q. Ye, R. Mo, and H. Li, "Low-frequency resonance suppression of a dual-active-bridge DC/DC converter enabled DC microgrid," *IEEE J. Emerg. Sel. Topics Power Electron.*, vol. 5, no. 3, pp. 982–994, Sep. 2017.

[32] PSIM Tutorial: How to use the lithium-ion battery model, 2017. [Online]. Available: http://www.powersimtech.com/wp-content/uploads/2013/04/Tutorial-How-to-use-Lithium-Ion-battery-model.pdf

[33] J. C. Hernandez, A. Medina, and F. Jurado, "Power quality assessment of current electrical vehicle charging processes," in *Proc. 2016 IEEE Asia-Pac. Power Energy Eng. Conf.*, 2016, pp. 1523–1527.

Authors' photographs and biographies not available at the time of publication.